Journal of Cranio-Maxillo-Facial Surgery 47 (2019) 661–667

Contents lists available at ScienceDirect

Journal of Cranio-Maxillo-Facial Surgery

journal homepage: www.jcmfs.com

Enhancing adhesion and alignment of human gingival fibroblasts on dental implants☆

Oral Cenk Aktas [a, 1], Wolfgang Metzger [b, 1], Ayman Haidar [c], Yahya Açil [d], Aydin Gülses [d], Jörg Wiltfang [d], Catharina Marques Sacramento [e], Frank Philipp Nothdurft [c, *]

[a] Institute for Materials Science, Christian-Albrechts-University Kiel, Germany
[b] Department of Trauma, Hand and Reconstructive Surgery, Saarland University, Homburg, Saar, Germany
[c] Department of Prosthetic Dentistry and Dental Materials Sciences, Saarland University, Homburg, Saar, Germany
[d] Department of Oral and Maxillofacial Surgery, Christian-Albrecht-Universität zu Kiel, Kiel, Germany
[e] Department of Prosthesis and Periodontology, Division of Periodontics, Piracicaba Dental School, University of Campinas, Piracicaba, Brazil

ARTICLE INFO

Article history:
Paper received 5 December 2018
Accepted 4 February 2019
Available online 21 February 2019

Keywords:
Dental implant
Nanogroove
Laser
Etching
Mechanical structuring

ABSTRACT

Background: Promoting the directional attachment of gingiva to the dental implant leads to the formation of tight connective tissue which acts as a seal against the penetration of oral bacteria. Such a directional growth is mostly governed by the surface texture.
Material and methods: In this study, three different methods, mechanical structuring, chemical etching and laser treatment, have been explored for their applicability in promoting cellular attachment and alignment of human primary gingival fibroblasts (HGFIBs).
Results: The effectiveness of mechanical structuring was shown as a simple and a cost-effective method to create patterns to align HGIFIBs.
Conclusion: Combining mechanical structuring with chemical etching enhanced both cellular attachment and the cellular alignment.

1. Introduction

Long-term performance of oral implants is governed by the formation and the preservation of healthy tissues around them (Welander et al., 2008). Excessive bacterial plaque development is one of the common problems leading to the inflammation of the soft tissue surrounding oral implants (Guida et al., 2013). When such a condition is left untreated, it may cause the destruction of the tissue supporting the implant (peri-implantitis) which may even end up with implant failure at late stages (Broggini et al., 2006).

Various successful therapeutic approaches have been reported for the prevention and treatment of peri-implantitis (Busscher et al., 2010). In addition, some novel implant surfaces have been developed for the prevention of peri-implantitis (Hoyos-Nogués et al., 2017). Such surfaces can be grouped in two main types. The first type is the *passive surface*, which exhibits an anti-bioadhesive nature due to their low surface energy (Mandracci et al., 2016). The second type is the *active surface*, which basically releases antimicrobial agents. On the other hand, the release of anti-microbial agents such as Ag^{+}, Cu^{2+} or similar ions leads to a delay in the osseointegration and it is still a challenge to control the release in terms of the delivery time and the dosage (Shivaram et al., 2017).

In recent years, biomimetic surfaces which activate the directional attachment of gingiva have been reported as an alternative solution for the prevention of peri-implantitis (Kearns et al., 2013). The directional attachment of gingiva to tooth root leads to the formation of a tight epithelium cuff and connective tissue which act as a seal against the penetration of oral bacteria (Naoyuki et al., 2017). In contrast, the directional attachment of collagen fibers mostly run parallel with the surface of an implant and this forms a weaker transmucosal seal which is less able to resist against the penetration of oral bacteria (Kearns et al., 2013).

Fibroblasts are highly sensitive to the surface texture. Ryoo et al. showed that fibroblasts exhibit enhanced adhesion and

☆ **This work should be attributed to:** Institute for Materials Science, Christian-Albrechts-University Kiel, Germany and Department of Prosthetic Dentistry and Dental Materials Sciences, Saarland University, Homburg/Saar, Germany.

* Corresponding author. Department of Prosthetic Dentistry and Dental Materials Sciences, Saarland University, Homburg, Saar, Germany.
E-mail address: frank.nothdurft@uks.eu (F.P. Nothdurft).

[1] Both authors contributed equally.

https://doi.org/10.1016/j.jcms.2019.02.004
1010-5182/

proliferation on 1D nanostructures (10.1021/nn1018279). On the contrary, previously we have shown that fibroblasts exhibit unusual morphology on densely deposited Al_2O_3 nanowires. This shows that not only the morphology but also the distribution density of nanostructures on the substrate seem to play a role on the cellular response of fibroblasts (10.1088/1758-5082/2/3/035001). Fibroblasts especially exhibit directional attachment and alignment on groove-like structures (Dunn and Brown, 1986). Various studies have reported on the contact guidance and the alignment of fibroblasts by micro- and nanogrooves (Hunter et al., 1995). Especially microgrooves have been extensively used to control the directional attachment and proliferation of fibroblasts. On the other hand, microscaled structures associated with increased bacterial attachment and colonization due to the increase in the surface roughness (Rimondini et al., 1997). Therefore, nanogrooves may provide the advantage of both promoting guided attachment and avoiding bacterial colonization. Various methods have been demonstrated to fabricate nanogrooves but most of these methods are composed of complicated multi-step processes and applicable only to planar substrates and small-areas (μm^2 to mm^2) (van Delft et al., 2008; Li et al., 2011). On the other hand, large-area and 3D structuring are compulsory for real implant applications.

In the present study, we compared the applicability of mechanical structuring, etching and laser surface treatment to dental implant materials for controlling the attachment and guidance of human primary gingival fibroblasts (HGFIBs). Linearly patterned (mechanically) titanium (Ti) surfaces have been etched mildly to achieve the combination of nanogrooves and randomly distributed nanostructures. After a detailed material analysis, we compared the effect of the dual-treated surface (nanogroove and random nanostructures) on adhesion, proliferation, and morphology of HGFIBs. We applied laser assisted surface peeling to eliminate nanogrooves from mechanically structured surfaces for comparing the cellular response on randomly distributed and aligned nanostructures. A special attention has been given to achieve a comparable roughness with mechanically structured/etched surfaces to distinguish the effect of the aligned and random nanostructures on the cellular attachment.

2. Materials and methods

2.1. Preparation of Surfaces

Commercially available titanium alloy Ti-6Al-4V samples (Goodfellow Materials Ltd.) with a thickness of 3 mm were cut from cylindrical bars (10 mm in diameter). Afterwards, samples were roughened (uniaxial) with SiC abrasive papers (CARBIMET PSA 500-Grit size of 500, Buehler) using alumina suspension (MicroPolish II Suspension-0.3 μm, Buehler) in a preparation system (TegraPol 31, Struers GmbH) in order to get a linear groove-like structures based on an optimized protocol (Ferraris et al., 2017). After a polishing/roughening process, samples were washed in acetone and distilled-deionized (DD) water, in an ultrasonic bath, in order to remove any surface contamination.

Prior to the etching, mechanically structured substrates were chemically treated by dipping them in a solution of HF (0.12 mol/L) and HNO_3 (0.08 mol/L) at room temperature for 15 min, and then dried in an oven at 45 °C for 24 h. Afterwards, samples were treated with a concentrated acid solution composed of HCl (5.80 mol/L) and H_2SO_4 (8.50 mol/L H_2SO_4) at 80 °C for 60 min and dried in an oven at 45 °C for 24 h.

For laser structuring a fiber-laser system (JK100FL) operating at a wavelength of 1080 ± nm was used in combination with a focusing element. The size of the focused laser beam was set to 1 mm. The mean laser energy output was kept about 25 W at a pulse rate of 50 Hz and a pulse period of 20 msec. Samples were moved under the stationary laser beam by a computer-controlled XY stage at a fixed scanning speed of 200 μm/s.

2.2. Surface Characterization

After the structuring, samples were cleaned using 70% ethanol and dried in air for 2 h. In order to perform scanning electron microscopy (SEM) first samples were sputtered with a thin gold layer (approx. 10 nm thick) using a physical vapor deposition (PVD) coater (JEOL-JFC-1300) and then they were mounted on SEM plates with a conductive adhesive carbon tape (Plano). A JEOL-JSM SEM was used to image the morphology of the samples. The images were taken at an accelerating voltage of 10 kV.

The surface roughness of the samples was measured by atomic force microscopy (AFM, TopoMetrix Explorer TMX 2000) equipped with a scanning stage of 200 μm × 200 μm. Samples were measured in both longitudinal and transversal directions. In order to analyze the wettability of the surfaces, static contact angle measurements were performed using a semi-automated contact angle meter (Krüss G2). Distilled-deionized (DD) water was used for all experiments. Three readings on a static sessile drop were taken for every substrate.

2.3. HGFIB in vitro cell culture

HGFIBs were purchased from Provitro AG (Lot-No. 230R290312, adult, Caucasian, male, passage 2) and were cultivated in fibroblast growth medium (Provitro). Cells were cultured under standard incubation parameters of 37 °C, 95% humidity and 5% CO_2. A maximum passage number of seven was used at a confluency of approx. 80%. Standard trypsinization procedures were used to detach the cells (Kiefer et al., 2016). In order to obtain defined cell numbers for seeding, the cell number was determined using a hemocytometer and the mean value was calculated. All cell culture experiments were performed in 24-well-plates. The different substrates were sterilized by rinsing them first with ethanol and water to eliminate any organic contamination prior to heating them in a special oven at 200 °C for 3 h. Following this, cells were seeded at a density of 200 cells/mm^2 onto the substrates and were cultivated until day 1 or day 3, respectively.

2.4. Determination of Cellular Viability and Cytotoxicity

For the determination of the cellular viability, we used the WST-1 assay (Cell Proliferation Reagent; Roche Diagnostics). Simultaneously, the Cytotoxicity Detection Kit^{PLUS} (Lactate Dehydrogenase (LDH) assay, Roche Diagnostics) was used for the determination of cytotoxicity. Samples were cultured as described before. At day 1 or day 3, the supernatant medium from each sample was transferred to an Eppendorf reaction tube to proceed with the LDH assay and the substrates with adhering HGFIBs were transferred into a new plate and washed once with phosphate buffered saline (PBS). Afterward cell viability was determined using WST-1 assay. This assay measures the formation of formazan by quantification of absorption at $\lambda = 420–480$ nm. Cell viability was ascertained after addition of WST-1 reagent and formazan formation was measured according to manufacturer's instruction manual. Two internal controls have been used for both assays. The mean absorbance of cells grown on control substrate was defined as 100% in the WST-1 assay, and the absorbance of the substrate cultivated cells was related to this value. For the LDH assay cells lysed by incubation in Triton X-100 (2%) were used as positive control (TX), exhibiting the maximum release of LDH and serving as a negative control.

For the LDH assay, the collected media were centrifuged at 1000 g for 5 min to eliminate the debris and the supernatants were

again transferred to new Eppendorf reaction tubes. A 100 μl of LDH substrate was added to a 100 μl of each sample and the formazan formation was measured as described in the manufacturer's instruction manual. The mean absorbance of 2% Triton X-100 treated cells was defined as 100%, and the absorbance of cells grown on the different substrates was related to this value. For each experiment, five different sets were repeated.

2.5. Analysis of Cellular Adhesion and Behavior

Immunohistochemical staining was used in order to observe the cellular adhesion and behavior. Both, the cytoskeletal F-actin and the focal adhesion-associated protein vinculin were stained. Accordingly, HGFIBs were cultivated as described before. At day 1 and day 3, the samples were washed once with PBS, fixed with 4% paraformaldehyde in PBS (PFA; Sigma–Aldrich) and permeabilized using 0.1% Triton X-100 solution in PBS (Carl Roth). After blocking with 1% bovine serum albumin in PBS (BSA; Sigma–Aldrich) the primary antibody against vinculin (Millipore) was added for 1 h. Following different washing steps, the samples were incubated with AlexaFluor488 labeled phalloidin for visualization of F-actin (Life Technologies, Darmstadt, Germany) and an AlexaFluor545 secondary antibody for visualization of vinculin (Life Technologies, Darmstadt, Germany). After washing twice with PBS, the cells were covered with ProLong® Gold antifade reagent including DAPI for nuclear counter staining (Invitrogen). The microscopic analysis was performed using a Zeiss Axioskop 2 fluorescence microscope equipped with the Axiovision software (Carl Zeiss).

2.6. Cell Counting

The number of cells on the substrates were quantified by counting DAPI-stained nuclei. As described before HGFIB nuclei were stained by ProLong® Gold antifade reagent including DAPI (Invitrogen). Ten separated visual fields pattern were identified for each sample and observed at 100× magnification under the fluorescence microscope. Seven different sets were repeated. Results were presented as a percentage of the mean from each surface.

2.7. Characterization of Cellular Morphology

The morphology of HGFIBs and their distribution on the different surfaces were analyzed by SEM. Cells were cultivated as mentioned before. At day 1 and day 3, media were discarded and substrates were washed with PBS. Fixation was done with 2% glutaraldehyde in 0.1 M sodium cacodylate buffer (pH 7.4) for 15 min at room temperature under slight movement. Afterward, the cells were contrasted using 1% osmium tetroxide (OsO_4) in 0.2 M sodium cacodylate buffer for 1 h in the dark. Then they were washed several times with DD water to eliminate any OsO_4 contamination. After the dehydration with increasing concentrations of ethanol, the cells were finally dried using hexamethyldisilazane (HMDS) and sputtered 3 times with gold for 60 s each (Sputter Coater SC 7640, Quorom Technologies). The specimens were examined with an FEI XL 30 ESEM FEG (FEI) SEM at 10 kV using secondary electron mode.

2.8. Statistical Analysis

Results for cell count, cell viability, and cytotoxicity tests were statistically analyzed in terms of significant ($p < 0.05$) and highly significant ($p < 0.01$) differences by applying a one-way ANOVA followed by a Student–Neuman–Keuls test for post-hoc analysis. The SigmaPlot- Software Version 11.0 (Systat) software was used to perform the analysis.

3. Results

3.1. Surface Characterization

Surface morphology was investigated by SEM. Fig. 1 shows SEM images of mechanically structured (MS), mechanically structured-chemically etched (MS-CE) and mechanically structured-laser treated (MS-LT) Ti surfaces. One can see aligned grooves on the surface of the MS Ti sample in Fig. 1a. We applied a custom method reported by Ferraris et al. for grinding and polishing Ti samples in order to get highly oriented nanoscaled grooves (Ferraris et al., 2017). At a closer look (Fig. 1d) grooves seem to have some discontinuities such as nanoscaled steps and protrusions. Following the etching, we observed the formation of additional finer structures which were randomly distributed on the Ti surface (Fig. 1b). Beside such randomly distributed nanoscaled structures, groove like linear structures from mechanical structuring persisted. These groove-like structures could be easier seen at higher magnifications (Fig. 1e). On the other hand, such grooves were not clearly seen unless a higher magnification was applied (Fig. 1e). To prepare a third type of surface, we applied laser treatment on MS Ti samples. Basically, Ti sample was scanned under a laser beam (operating at a wavelength of 1085 nm and power of 25 W) at a scanning speed of 200 μm/s. Fig. 1c shows a typical morphology of a laser treated surface and at a closer look (Fig. 1f) one can see that nanostructured topography consists of protrusions and hill-lock type structures formed upon the fast melting-solidification cycle.

The custom developed grinding and the polishing protocol was optimized in order to get a transversal roughness (R_a) of about 78 ± 4 nm (perpendicular to nanogrooves) on MS Ti samples (Fig. 2a). Such grooves exhibited typically heights in the range 250–300 nm while their widths vary between 85 nm and 420 nm. After etching the surface, the transversal roughness (perpendicular to nanogrooves) increased slightly ($R_a = 92 \pm 5$ nm). As we aimed we achieved a roughness comparable to that of MS-CE surface after the laser treatment (transversal $R_a = 88 \pm 4$ nm). Aqueous wettability of prepared surfaces was analyzed by the static contact angle (CA) measurement. While MS surface exhibited a CA of 63 ± 4, this value increased to 87 ± 3 after etching. On the other hand, after laser treatment, we achieved a quite good wetting which is proven by a CA of 5 ± 2. While we observed a significant difference in transversal and longitudinal roughness of MS and MS-CE surfaces, MS-LT surface exhibited nearly identical values in both directions.

3.2. Cytotoxicity and Metabolic activity

LDH-assay and WST-1 (Fig. 3a, b) assay were performed to reveal the cytotoxicity and metabolic activity of HGFIBs on prepared surfaces, respectively. At day 1 MS and MS-CE surfaces indicated low cytotoxicity levels in comparison to the TX sample serving as a cytotoxic positive control. MS-LT surface showed a 40% toxicity level compared to TX, indicating a higher cytotoxicity with respect to MS and MS-CE surfaces. A similar trend was observed after day 3, but with a general higher percentage of cytotoxicity compared to day which is proportionally related to the higher density of the HGFIBs. Regarding HGFIB proliferation, MS surface was taken as the positive control with 100% metabolic activity. At day 1, it is observed that HGFIBs proliferation on MS-CE surface was similar to that observed on MS surface, while almost 20% less proliferation was observed on MS-LT surface. At day 3, HGFIBs proliferation on MS-CE surface increased slightly compared to MS surface. On the other hand, HGFIB proliferation on MS-LT surface decreased and a significant difference ($p < 0.01$) of 35% less HGFIB proliferation was observed in comparison to that of MS surface.

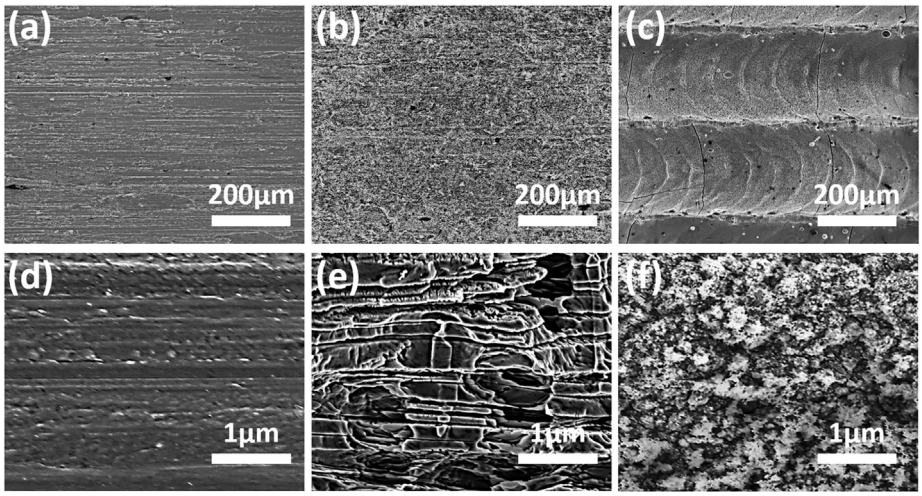

Fig. 1. SEM images of **(a)** MS surface, **(b)** MS-CE surface and **(c)** MS-LT surface. Corresponding higher magnifications are given in **(d)**, **(e)** and **(f)**, respectively.

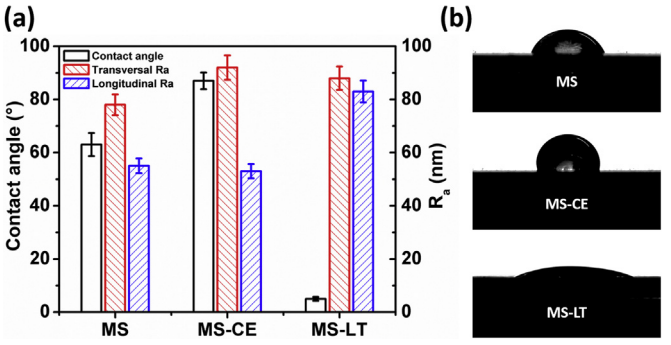

Fig. 2. **(a)** CA and roughness (longitudinal and transversal directions) analysis of prepared surfaces and **(b)** Optical images of sessile water drops on prepared surfaces (Transversal positioned).

3.3. Cell Adhesion and Proliferation

Fluorescence microscopy was used to reveal F-actin distribution in the cytoskeleton (green) and focal adhesion points represented by vinculin density (red) (Fig. 4a–f). After day 1 of cultivation, F-actin filaments were well distributed and formed a normal cytoskeleton on both MS and MS-CE surfaces without a significant indication of stress factors. We observed a clear alignment of HGFIBs on both surfaces. Relatively high vinculin density on MS-CE surface was a clear indication of well HGFIB adherence. On the other hand, HGFIB cultured on MS-LT surfaces exhibited much smaller and abnormal morphologies. Opposite to MS and MS-CE surfaces, neither a strong attachment nor a significant alignment of HGFIB has been observed on MS-LT surface. Low vinculin density was a clear sign of a poor HGFIB adhesion. At day 3, a higher density of HGFIB was observed on MS and MS-CE surfaces Actin filaments distributed in the cytoplasm and formed a healthy cytoskeleton. Alignments and orientation of HGFIB on MS and MS-CE surfaces became much stronger.

The HGFIBs density was quantified using nucleus count after DAPI staining. The percentage of the HGFIB count on prepared surfaces is presented graphically in Fig. 4g. HGFIB density on MS surface at day 1 is taken as 100% (as the reference substrate). At day 1, an HGFIB density increased by 36% on MS-CE surface whereas on MS-LT no significant difference was observed. At day 3, HGFIB density significantly decreased on MS-LT surface (37% less) compared to MS surface. MS-CE surface exhibited the highest cell density with almost 40% improvement in comparison to that observed on MS surface.

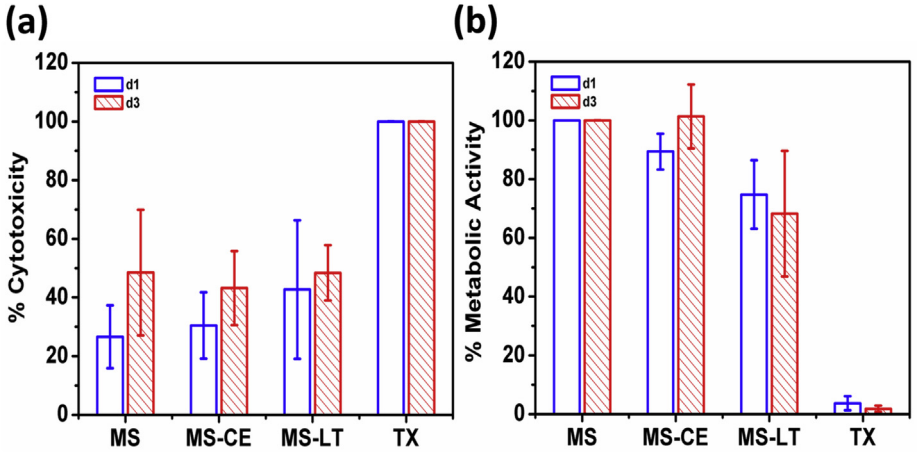

Fig. 3. **(a)** Cytotoxicity analysis (LDH assay) and **(b)** metabolic activity (WST-1 assay) analysis.

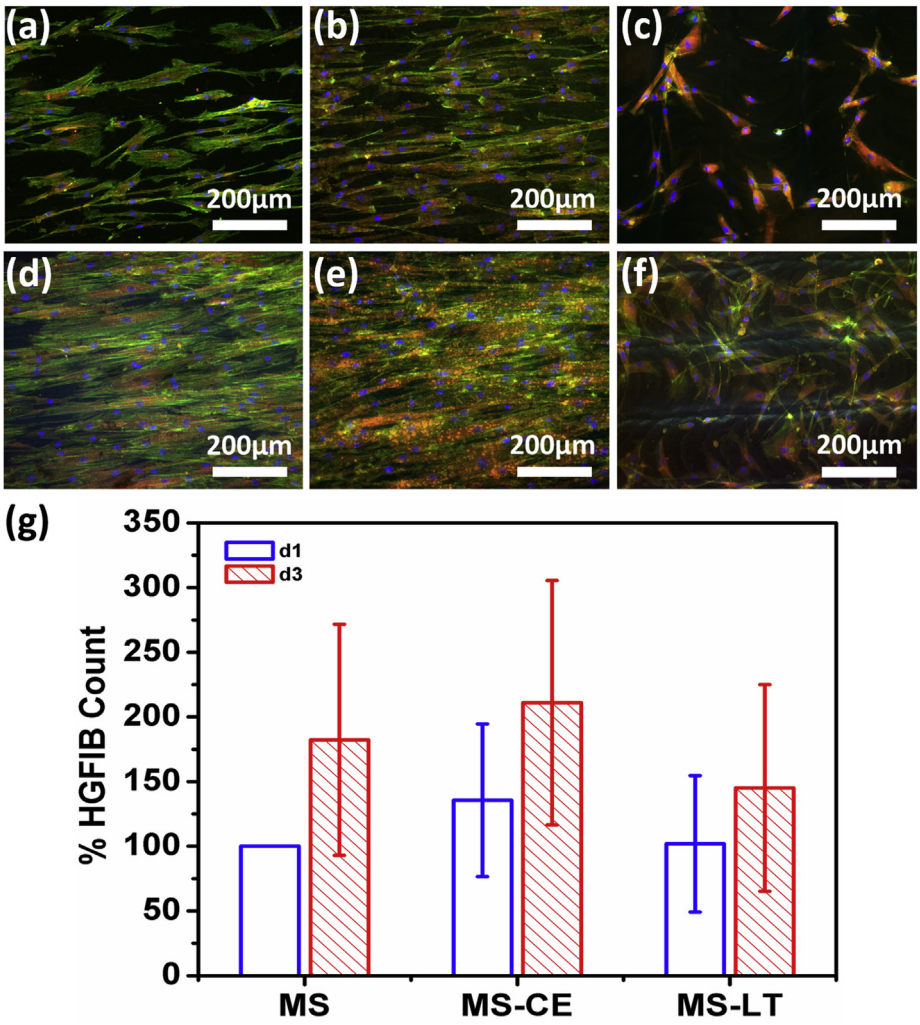

Fig. 4. Fluorescence microscopy images of stained HGFIBs cultured on **(a)** MS surface, **(b)** MS-CE surface and **(c)** MS-LT surface on day 1. Signals for vinculin can be seen in red, F-actin is stained green. Corresponding images recorded at day 3 are given in **(d)**, **(e)** and **(f)**, respectively. **(g)** HGFIB density on prepared surfaces.

3.4. Cellular Morphology

SEM analysis given in Fig. 5 presents a detailed morphology of the HGFIBs cultured on prepared surfaces. At day 1, HGFIBs showed a normal and healthy morphology on both MS and MS-CE surfaces. Additionally, HGFIBs showed an alignment and orientation on both surfaces. In contrast, HGFIB density and size were reduced on MS-LT surface and a chaotic distribution of HGFIB rather than any alignment was observed. It was clear that the HGFIBs were stressed by the formation of filopodia searching for a rough structure in order to try to attach and survive. After day 3 of incubation, a similar morphology and behavior of the HGFIB were observed on prepared surfaces as seen on day 1. HGFIBs exhibited better alignment, higher density and healthier morphology on MS and MS-CE surfaces. On day 3, the number of HGFIBs was quite less on MS-LT surface and the cell morphology remained similar to that observed on day 1 exhibiting low spread cells indicating problems to adhere properly.

4. Discussion

The effect of surface topography on gingival fibroblast attachment and alignment on micro-topographies has been reported by various research groups (Muñiz Maisonet et al., 2015; Oakley and Brunette, 1993). For many cell types, cells align to anisotropic microscale grooves, with larger features increasing the extent of alignment, up to a size limit above which cells do not respond (Ristori et al., 2016). On the other hand, it is known that microroughness triggers bacterial adhesion and accumulation, too (Lorenzetti et al., 2015). Therefore, nanotopography seems to be the right choice for promoting the alignment of fibroblasts while not promoting the bacterial adhesion and proliferation.

Various nanoscaled surface topographies have been developed using advanced materials processing technologies such as ion beam lithography, nanoimprint lithography, dip-pen lithography, direct laser interference patterning and many more (He et al., 2003; Schieber et al., 2017; Wang et al., 2017). Most of these methods are applicable to very small areas at the order of only a few mm^2. In addition, some of these methods are applicable only to some special materials (soft polymers, hydrogels, etc.) which cannot be used as an implant material due to the lack of mechanical strength and stability. The complexity (multi-step processes) and the high cost of such manufacturing methods also limit their use in clinical dentistry. Our study aimed to reveal the applicability of easy state of the art surface treatment methods to promote the attachment and proliferation of HGFIBs in a controlled manner, mimicking the gingival attachment to the tooth root. Basically, dental implant

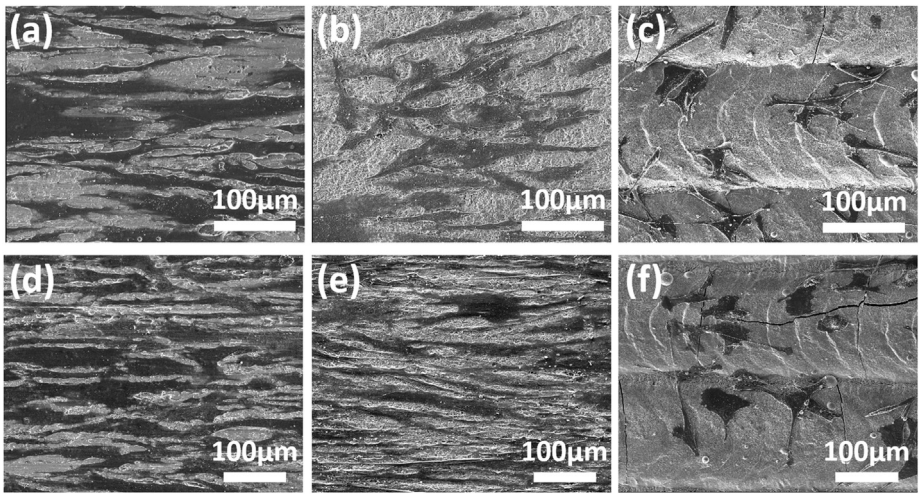

Fig. 5. SEM images of HGFIBs cultured on **(a)** MS surface, **(b)** MS-CE surface and **(c)** MS-LT surface on day 1. Corresponding images recorded at day 3 are given in **(d)**, **(e)** and **(f)**, respectively.

manufacturers prefer mechanical structuring, acid etching and laser treatment to modify implant surfaces.

Hot-rolled titanium naturally exhibits a groove structure due to the mechanical deformation. These defects structure defines the size of structures which can be created by micromachining. By using an optimal polishing procedure (concentric micromachining by the cutting tools with R_a below 250 nm) one can get nanogrooves with a dimension down to 10 nm (Davim and Jackson, 2009). Etching, in general, leads to the selective removal of the material from the surface leaving behind a micro- and nanostructured topography depending on the etchant type, etching medium, and environment. Double-etching method is quite a well-known process which has been accepted almost as a gold standard (Giner et al., 2017). In our study, we showed that etching mechanically structured Ti surfaces led to two kinds of morphologies: nanogrooves and random nanostructures. Both regular groove types and randomly distributed structures affect the wettability properties and this plays a major role on the protein adsorption and cellular interaction (Benni et al., 2014; Xu and Siedlecki, 2007).

In their pioneering work, Dalby et al. showed that cells can sense structures down to 13–15 nm (Dalby et al., 2003). Therefore, it is clear to us that our etched surface MS-CE which consists of nanoscale structures is able to promote cellular adhesion (Fig. 4g). On the other hand, randomly distributed nanoscaled surface structures are known not to promote contact guidance (cell alignment). Our study showed that directional structures were preserved after the mild etching. Therefore, the combination of randomly distributed nanostructures and aligned nanogrooves, promote both cellular adhesion and cell alignment. The surface hydrophobicity is well known to be a key factor to govern cell response. Basically, one can measure the CA of a water droplet spreading on a solid surface to reveal the hydrophobicity. There are various research works which demonstrated enhanced cell adhesion on hydrophilic surfaces (Wang et al., 2016; Webb et al., 1998). Fibroblasts were found to have maximum adhesion when CAs were between 60 and 80 (Tamada and Ikada, 1993). Interestingly, Vogler et al. showed that more hydrophilic surfaces with CAs <65 did not lead to higher cell attachment (Noh and Vogler, 2006). We do believe that at the micro- and nanoscale we have local wetting contrasts (hydrophobic and hydrophilic) due to non-homogenous surface topography. We presented such local changes in wetting on laser patterned surfaces previously (May et al., 2015). It has been shown that on non-homogenous nanoscaled structures one can observe a large contact-angle hysteresis which indicates the existence of an intermediate state between the Cassie–Baxter and Cassie–Wenzel models (Bormashenko, 2010). This means at the micro- and nanoscale, we possibly have such a transition (hydrophilic and hydrophobic regions) modulated by the linear surface structures and this may promote the cellular alignment. For instance, we do believe on MS-LT surface such a local wetting contrast does not exist (lack of linear structures) and therefore we did not observe any cell alignment. It is known that strong hydrophilic (water CAs below 10) surfaces are also known as protein repellent surfaces which may lead to the reduction in cellular attachment (Herrwerth et al., 2003).

Lasers have been used to texture the surface of medical implants. Previously we presented the modulation of the wetting angle on Ti surfaces by laser treatment. In this study, we used the laser for a different aim rather than micro-grooving the surface. In our previous study, we have observed that laser led to a local melting on the surface and a nanotopography formed upon fast solidification (Herrwerth et al., 2003). It has been demonstrated that even lasers can be used as an effective tool to polish metallic surfaces (Giorleo et al., 2015). Similar to that, here we used a laser to get rid of mechanically induced linear structures and to achieve a roughness similar to that of MS-CE surface. Actually, we could simply etch Ti surface for a longer time to get rid of nanogrooves, but then the roughness definitely would get much higher, which might hinder comparability of prepared surfaces in terms of cellular attachment and orientation. Although MS-LT surface exhibited nearly identical roughness with MS-CE surface, we did not detect any cellular alignment. Moreover, cell density decreased significantly on MS-LT surface which might be due to extremely low CA.

Our study shows that nanoscaled topography can enhance the cellular attachment of HGFIBs and one can control their alignment by inducing nanogroove like patterns on the substrate surface. On the other hand, surface chemistry needs to be explored to understand the underlying mechanism of the cellular attachment and alignment. Although our cytotoxicity analysis showed that all prepared surfaces are biocompatible still there is a need to get details of the surface in terms of functional groups and polarity.

5. Conclusion

Commercially available surface patterning methods, mechanical structuring, chemical etching and laser treatment have been

explored for their applicability in promoting cellular attachment and alignment of HGFIBs. Mechanical structuring led to an effective patterning on Ti implant surfaces and it can be used as a simple and a cost-effective method to create patterns on Ti implants to align HGFIBs. Combining mechanical structuring with chemical etching led to much improved cellular attachment while not disturbing the cellular alignment. It seems that while random nanoscaled structures promoted the adhesion of more HGFIBs, nanogrooves triggered the cellular alignment. It is believed that higher CAs achieved on MS and MS-CE surfaces also play an important role in terms of creating local (at the micro- and nanoscale) wetting contrasts on the surface supporting cellular alignment.

In contrast, random nanotopography as well as the absence of linear groove type of structures seem to suppress both cellular attachment and alignment of HGFIBs. This may be related to the extreme hydrophilicity of the surface and lack of any directional structures. Since none of the prepared samples exhibited a toxic nature, achieved surface chemistries seem to exhibit high biocompatibility. On the other hand, it is known that surface chemistry also plays a major role in the cellular response. Therefore, a detailed study is foreseen to compare the surface chemistries of structures prepared by the presented three methods.

Acknowledgements

This study was realized by using institutional funding (Department of Prosthetic Dentistry and Dental Materials Sciences, Saarland University). Author C.M.S. collaborated in this project as an exchange student supported by grant number 88888.099049/2013-00 from CAPES Foundation, Ministry of Education of Brazil, Brasília.

Appendix A. Supplementary data

Supplementary data to this article can be found online at https://doi.org/10.1016/j.jcms.2019.02.004.

References

Benni S, Avramoglou T, Hlawaty H, Mora L: Dynamic Contact Angle Analysis of Protein Adsorption on Polysaccharide Multilayer's Films for Biomaterial Reendothelialization. BioMed Res Int: 1–10, https://doi.org/10.1155/2014/679031

Bormashenko E: Wetting transitions on biomimetic surfaces. Phil Trans R Soc A 368: 4695–4711, https://doi.org/10.1098/rsta.2010.0121; 2010

Broggini N, McManus LM, Hermann JS, Medina R, Schenk RK, Buser D, et al: Periimplant Inflammation Defined by the Implant-Abutment Interface. J Dent Res 85(5): 473–478, https://doi.org/10.1177/154405910608500515; 2006

Busscher HJ, Rinastiti M, Siswomihardjo W, van der Mei HC: Biofilm Formation on Dental Restorative and Implant Materials. J Dent Res 89(7): 657–665, https://doi.org/10.1177/0022034510368644; 2010

Dalby MJ, Childs S, Riehle MO, Johnstone HJH, Affrossman S, Curtis ASG: Fibroblast reaction to island topography: changes in cytoskeleton and morphology with time. Biomaterials 24(6): 927–935, https://doi.org/10.1016/S0142-9612(02)00427-1; 2003

Davim JP, Jackson MJ. In: Davim JP, Jackson MJ (eds), Nano and Micromachining. London, UK: ISTE, https://doi.org/10.1002/9780470611807; 2009

Dunn GA, Brown AF: Alignment of fibroblasts on grooved surfaces described by a simple geometric transformation. J Cell Sci 83: 313–340, 1986

Ferraris S, Truffa Giachet F, Miola M, Bertone E, Varesano A, Vineis C, et al: Nanogrooves and keratin nanofibers on titanium surfaces aimed at driving gingival fibroblasts alignment and proliferation without increasing bacterial adhesion. Mater Sci Eng C 76: 1–12, https://doi.org/10.1016/j.msec.2017.02.152; 2017

Giner L, Mercadé M, Torrent S, Punset M, Pérez RA, Delgado LM, et al: Double acid etching treatment of dental implants for enhanced biological properties. J Appl Biomater Funct Mater 16(2): 83–89, https://doi.org/10.5301/jabfm.5000376; 2017

Giorleo L, Ceretti E, Giardini C: Ti Surface Laser Polishing: Effect of Laser Path and Assist Gas. Procedia CIRP 33: 446–451, https://doi.org/10.1016/j.procir.2015.06.102; 2015

Guida L, Oliva A, Basile MA, Giordano M, Nastri L, Annunziata M: Human gingival fibroblast functions are stimulated by oxidized nano-structured titanium surfaces. J Dent 41(10): 900–907, https://doi.org/10.1016/j.jdent.2013.07.009; 2013

He W, Gonsalves KE, Batina N, Poker DB, Alexander E, Hudson M: Micro/nanomachining of Polymer Surface for Promoting Osteoblast Cell Adhesion. Biomed Microdevices 5(2): 101–108, 2003

Herrwerth S, Eck W, Reinhardt S, Grunze M: Factors that Determine the Protein Resistance of Oligoether Self-Assembled Monolayers – Internal Hydrophilicity, Terminal Hydrophilicity, and Lateral Packing Density. J Am Chem Soc 125(31): 9359–9366, https://doi.org/10.1021/ja034820y; 2003

Hoyos-Nogués M, Velasco F, Ginebra MP, Manero JM, Gil FJ, Mas-Moruno C: Regenerating Bone via Multifunctional Coatings: The Blending of Cell Integration and Bacterial Inhibition Properties on the Surface of Biomaterials. ACS Appl Mater Interfaces 9(26): 21618–21630, https://doi.org/10.1021/acsami.7b03127; 2017

Hunter A, Archer CW, Walker PS, Blunn GW: Attachment and proliferation of osteoblasts and fibroblasts on biomaterials for orthopaedic use. Biomaterials 16(4): 287–295, https://doi.org/10.1016/0142-9612(95)93256-D; 1995

Kearns VR, Williams RL, Mirvakily F, Doherty PJ, Martin N: Guided gingival fibroblast attachment to titanium surfaces: an in vitro study. J Clin Periodontol 40(1): 99–108, https://doi.org/10.1111/jcpe.12025; 2013

Kiefer K, Akpınar G, Haidar A, Ikier T, Akkan CK, Akman E, et al: Al2O3 micro- and nanostructures affect vascular cell response. RSC Advances 6(21): 17460–17469, https://doi.org/10.1039/C5RA21775J; 2016

Li K, Morton K, Veres T, Cui B: Nanoimprint Lithography and Its Application in Tissue Engineering and Biosensing. In: Comprehensive Biotechnology, 2nd ed., https://doi.org/10.1016/B978-0-08-088504-9.00497-9; 2011

Lorenzetti M, Dogša I, Stošicki T, Stopar D, Kalin M, Kobe S, et al: The Influence of Surface Modification on Bacterial Adhesion to Titanium-Based Substrates. ACS Appl Mater Interfaces 7(3): 1644–1651, https://doi.org/10.1021/am507148n; 2015

Mandracci P, Mussano F, Rivolo P, Carossa S: Surface Treatments and Functional Coatings for Biocompatibility Improvement and Bacterial Adhesion Reduction in Dental Implantology. Coatings 6(1): 7, https://doi.org/10.3390/coatings6010007; 2016

May A, Agarwal N, Lee J, Lambert M, Akkan CK, Nothdurft FP, et al: Laser induced anisotropic wetting on Ti–6Al–4V surfaces. Mater Lett 138: 21–24, https://doi.org/10.1016/j.matlet.2014.09.092; 2015

Muñiz Maisonet M, Elineni KK, Toomey RG, Gallant ND: Combining Nonadhesive Materials into Microstructured Composite Surfaces Induces Cell Adhesion and Spreading. ACS Biomater Sci Eng 1(11): 1163–1173, https://doi.org/10.1021/acsbiomaterials.5b00309; 2015

Naoyuki K, Akasaka T, Horiuchi R, Yoshida Y, Yokoyama A: Cell adhesion and alignment of human osteoblasts and human gingival fibroblasts on micro/nano-grooved gelatin sheet. Digest J Nanomater Biostruct 12(2): 431–440, 2017

Noh H, Vogler EA: Volumetric interpretation of protein adsorption: Mass and energy balance for albumin adsorption to particulate adsorbents with incrementally increasing hydrophilicity. Biomaterials 27(34): 5801–5812, https://doi.org/10.1016/j.biomaterials.2006.08.005; 2006

Oakley C, Brunette DM: The sequence of alignment of microtubules, focal contacts and actin filaments in fibroblasts spreading on smooth and grooved titanium substrata. J Cell Sci 106(1): 343–354, 1993

Rimondini L, Faré S, Brambilla E, Felloni A, Consonni C, Brossa F, et al: The Effect of Surface Roughness on Early In Vivo Plaque Colonization on Titanium. J Periodontol 68(6): 556–562, https://doi.org/10.1902/jop.1997.68.6.556; 1997

Ristori T, Vigliotti A, Baaijens FPT, Loerakker S, Deshpande VS: Prediction of Cell Alignment on Cyclically Strained Grooved Substrates. Biophys J 111(10): 2274–2285, https://doi.org/10.1016/j.bpj.2016.09.052; 2016

Schieber R, Lasserre F, Hans M, Fernández-Yagüe M, Díaz-Ricart M, Escolar G, et al: Direct Laser Interference Patterning of CoCr Alloy Surfaces to Control Endothelial Cell and Platelet Response for Cardiovascular Applications. Adv Healthc Mater 6(19): 1700327, https://doi.org/10.1002/adhm.201700327; 2017

Shivaram A, Bose S, Bandyopadhyay A: Understanding long-term silver release from surface modified porous titanium implants. Acta Biomater 58: 550–560, https://doi.org/10.1016/j.actbio.2017.05.048; 2017

Tamada Y, Ikada Y: Effect of Preadsorbed Proteins on Cell Adhesion to Polymer Surfaces. J Colloid Interface Sci 155(2): 334–339, https://doi.org/10.1006/jcis.1993.1044; 1993

van Delft JM, van den Heuvel FC, Loesberg WA, te Riet J, Schön P, Figdor CG, et al: Manufacturing substrate nano-grooves for studying cell alignment and adhesion. Microelectron Eng 85: 1362–1366, https://doi.org/10.1016/j.mee.2008.01.028; 2008

Wang LS, Duncan B, Tang R, Lee YW, Creran B, Elci SG, et al: Gradient and Patterned Protein Films Stabilized via Nanoimprint Lithography for Engineered Interactions with Cells. ACS Appl Mater Interfaces 9(1): 42–46, https://doi.org/10.1021/acsami.6b13815; 2017

Wang W, Caetano G, Ambler W, Blaker J, Frade M, Mandal P, et al: Enhancing the Hydrophilicity and Cell Attachment of 3D Printed PCL/Graphene Scaffolds for Bone Tissue Engineering. Materials 9(12): 992, https://doi.org/10.3390/ma9120992; 2016

Webb K, Hlady V, Tresco PA: Relative importance of surface wettability and charged functional groups on NIH 3T3 fibroblast attachment, spreading, and cytoskeletal organization. J Biomed Mater Res 41(3): 422–430, 1998 https://doi.org/10.1002/(SICI)1097-4636(19980905)41:3<422::AID-JBM12>3.0.CO;2-K

Welander M, Abrahamsson I, Berglundh T: The mucosal barrier at implant abutments of different materials. Clin Oral Implants Res 19(7): 635–641, https://doi.org/10.1111/j.1600-0501.2008.01543.x; 2008

Xu LC, Siedlecki CA: Effects of surface wettability and contact time on protein adhesion to biomaterial surfaces. Biomaterials 28(22): 3273–3283, https://doi.org/10.1016/j.biomaterials.2007.03.032; 2007